Available online at www.sciencedirect.com

ScienceDirect

Procedia Structural Integrity 28 (2020) 648–658

Structural Integrity Procedia

www.elsevier.com/locate/procedia

1st Virtual European Conference on Fracture

Tensile and fatigue behavior of a Pb-Sn-Sb alloy investigated via small-scale *in-situ* mechanical testing in SEM

Di Wan[a,*], Luigi Mario Viespoli[a], Audun Johanson[b], Anette Brocks Hagen[c], Filippo Berto[a], Antonio Alvaro[a,c]

[a]*Department of Mechanical and Industrial Engineering, Norwegian University of Science and Technology, Richard Birkelands vei 2B, 7491 Trondheim, Norway*

[b]*Nexans Norway, Innspurten 9, 0663 Oslo, Norway*

[c]*Department of Materials Integrity and Welding, SINTEF Industry, 7456 Trondheim, Norway*

Abstract

Pb-Sn-Sb alloys (E-alloy) are commonly used in subsea power cable sheathing. Due to the relatively low melting temperature, *i.e.* around 600 K, this type of alloy is prone to experience microstructural time-dependent evolution such as recovery, relaxation, recrystallization and creep deformation even at room temperature, in contrast to other conventional materials for which involve these mechanisms are activated only at high temperatures. To better understand the deformation mechanisms of Pb-Sn-Sb alloys, small-scale *in-situ* mechanical testing inside a scanning electron microscope (SEM) has been conducted under both monotonic loading and cyclic loading conditions. Thanks to the *in-situ* imaging technique, the deformation behavior as well as the damage mechanisms were revealed with high resolution. The possible deformation mechanisms, including the creep behavior, has been discussed and the results can provide necessary input to damage calculations and modelling work of the studied alloy system used for cable sheathing.

Keywords: Pb-Sn-Sb alloy; creep; fatigue; *in-situ* test; SEM.

* Corresponding author.
E-mail address: di.wan@ntnu.no

2452-3216
10.1016/j.prostr.2020.10.075

1. Introduction

Lead alloys are commonly used in subsea cable sheathing due to their easy manufacturing, excellent chemical stability and mechanical ductility [1, 2]. A common understanding of this material is that due to its low melting point (~600 K or 327 °C), the deformation behavior includes relaxation, recovery, recrystallization or creep even at room temperature, in contrast to conventional metallic materials which experience these behaviors only at high temperatures. These time-dependent phenomena lead to a sensitive strain rate-dependency of lead alloys in terms of the constitutive behavior and damage during deformation. The real-life scenarios involving cyclic motion will both vary in strain rate and entail cycles with strain rates far below practical limits if testing due to time constraints, *i.e*. it is a clear need to better understand the inherent damage models in order to improve the necessary extrapolations needed for fatigue- and creep damage calculations. Due to the complexity of the issue, the industry has for long time relied on the experience derived from the operational history rather the inadequate available literature on the topic. Among the earlier works we mention an investigation by the University of Illinois of the mechanical behavior of lead for cable sheathing at a range of temperatures, showing a strong strain rate dependency on the evolution of the plastic curve and on the tensile strength [3] and a study on the impact of chemical composition of the alloy, thermal treatments and repeated loading [4]. The impact of grain size on the creep behavior of polycrystalline lead was studied by Feltham [5] while tests on the fatigue behavior of commercial alloys were performed by Harvard [6]. Further works are available on the fatigue behavior [7] and the compression response [8]. Being most of the research available is outdated and inadequate to understand real life fatigue calculations, as well as significant manufacturing and cable design improvements, a novel interest for the performance of lead alloys has risen in the industry. In the recent years novel results have been produced with up to date tools, describing the tensile performance and the fatigue response in presence of geometrical discontinuities of a selection of lead alloys of interest [9-11], together with a statistical estimation of the sheathing's life in full scale tests [1]. The present work aims to present some interesting preliminary result to expand and improve the understanding of the mechanisms leading to failure under various loading conditions.

2. Materials and Experimental

The material investigated in this study is a Pb-Sn-Sb alloy (E-alloy) with the chemical composition shown in Table 1. The material was extracted from as-extruded lead tubes which involve direct quenching upon extrusion. Followed by > 1 year of storage. The as-received material has a face-centered cubic (FCC) phase with a small fraction of secondary precipitates (identified as SnSb particles by energy dispersive X-ray spectroscopy/ EDX) and was manufactured into dog-bone shaped tensile specimens with the dimension described in Figure 1 with the longitudinal direction parallel to the extruded direction of the raw material. The metallographic investigation of this material can be found in Ref. [11]. The specimens are prepared by grinding, polishing, etching and ion-polishing at 2 kV for 10 min plus 1 kV for 10 min. Before testing, the specimen was analyzed by electron backscatter diffraction (EBSD) technique in a Quanta 650 FEG scanning electron microscope (SEM, ThermoFisher Inc., USA) with an accelerating voltage of 20 kV and a working distance of about 15 mm. The initial microstructure of the material as revealed through EBSD maps is shown in Figure 2. An average grain size of about 25 μm is observed, and the grains are mostly in equiaxed shape. No specific sharp texture is observed from the normal direction - inverse pole figure (ND-IPF) map. A lot of twin boundaries (TBs, defined by Σ3 boundaries) together with low-angle grain boundaries (LAGBs, 2-15°) and high-angle grain boundaries (HAGBs, >15°) are revealed by the EBSD analysis. The residual strain after sample preparation revealed by kernel average misorientation (KAM, defined as the average misorientation of first nearest points including the kernel scanning point) map is not significantly strong. The specimen was considered as in well-annealed state before testing.

Table 1 Chemical composition of the tested material.

Element	Pb	Sb	Sn
wt.%	99.3	0.2	0.5

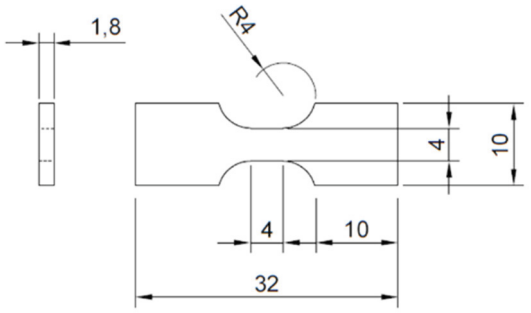

Figure 1 Sample geometry for tensile testing. (unit: mm)

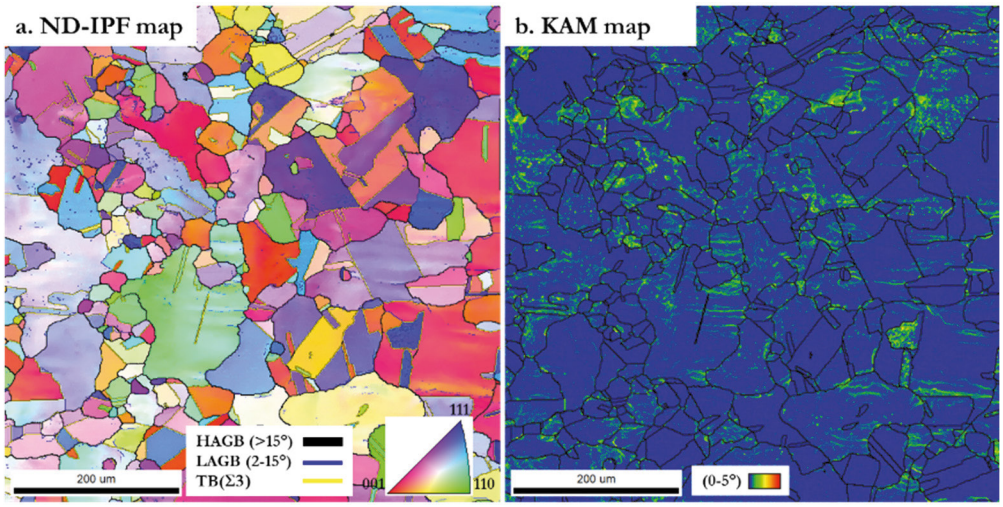

Figure 2 EBSD analysis of the tested material: a. normal direction - inverse pole figure (ND-IPD) map with high-angle grain boundaries (HAGBs), low-angle grain boundaries (LAGBs) and twin boundaries (TBs, defined by Σ3 boundaries), b. kernel average misorientation (KAM) map with 0-5°. (digital version in color)

Mechanical loading was applied by a tensile/compression module (Kammrath & Weiss GmbH, Germany) inside the SEM. Monotonic tensile tests with an initial nominal strain rate of from 5×10^{-5} s^{-1} to 5×10^{-3} s^{-1} were performed. For cyclic loading test, a nominal strain amplitude ($\Delta\varepsilon$) of approx. ±1.1% with an initial nominal strain rate of 5×10^{-3} s^{-1} was applied. The deformation procedure of specimens was recorded by *in-situ* SEM imaging at a chosen magnification to reveal the microstructural change during testing. Energy dispersive X-ray spectroscopy (EDS) was used to confirm the chemical composition information of the specimen at an accelerating voltage of 20 kV and a working distance of about 10 mm. The post-mortem fracture features were also investigated by SEM to confirm the fracture mechanism.

3. Results

3.1. Mechanical data

3.1.1 Monotonic loading

Figure 3 shows the nominal stress – strain curves for monotonic tensile tests on three different specimens with different nominal strain rates. The first two tests were done with a fixed nominal strain rate at 5×10^{-3} s^{-1} and 5×10^{-4} s^{-}

[1], respectively (referring to the black and the red curves). The third test was started with 5×10^{-5} s^{-1} but accelerated after the ultimate tensile strength has been clearly passed (*i.e.* after a clear drop in the nominal stress has been recorded). The accelerated testing ranges are divided by black dashed lines in Figure 3 and the corresponding nominal strain rates are marked accordingly. It is clear that the mechanical properties of the studied Pb-Sn-Sb alloy have a strong dependency on the strain rate. The yield strength (by 0.2% plastic deformation criterion) as well as the ultimate tensile strength increases with an increasing strain rate, and these values are recorded in Table 2. An interesting fact is that the final elongation/ nominal strain is quite similar (about 110%) between the different testing cases.

Table 2 Mechanical properties of the tested Pb-Sn-Sb alloy.

Nominal strain rate / s^{-1}	Yielding strength/ MPa	Ultimate tensile strength/ MPa
$5\times10^{-5,*}$	8.2	16.1
5×10^{-4}	8.8	17.4
5×10^{-3}	10.8	20.7

*The properties for 5×10^{-5} s^{-1} were got from the first segment of the blue curve in Figure 3.

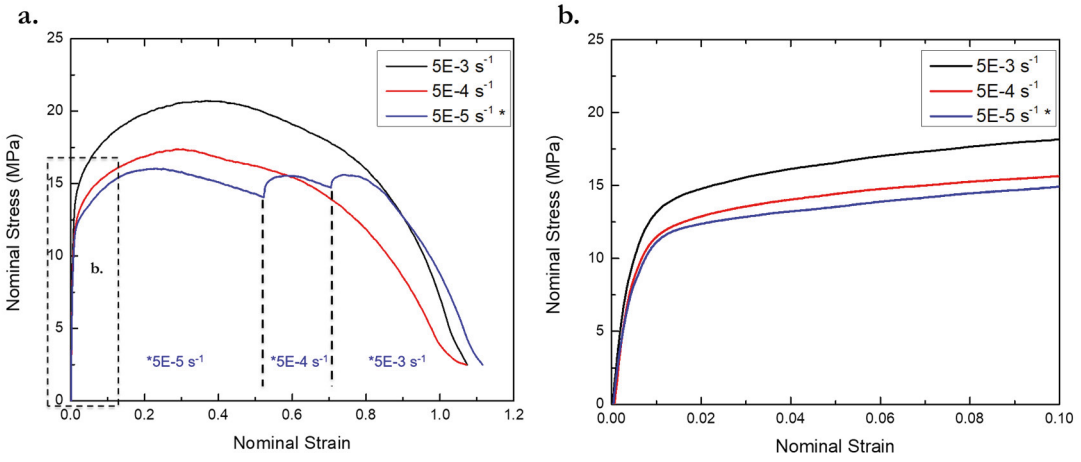

Figure 3 a. Nominal stress – strain curves for monotonic loading tests with strain rates ranging from 5×10^{-5} s^{-1} to 5×10^{-3} s^{-1}. The black and red curves were from the tests with a fixed strain rate at 5×10^{-3} s^{-1} and 5×10^{-4} s^{-1}, respectively. The blue curve started with 5×10^{-5} s^{-1}, and the loading was accelerated after the drop in the stress has been recorded. The segments are divided by black dashed lines and the corresponding nominal strain rates are marked. b. A magnified area focusing on the first stage of deformation (nominal strain less than 0.1). (digital version in color)

3.1.2 Cyclic loading

The cyclic loading test was conducted under an elongation-controlled mode with a fixed displacement rate (corresponding to an initial nominal strain rate of 5×10^{-3} s^{-1}). The corresponding global strain amplitude was $\Delta\varepsilon \sim \pm1.1\%$. The testing results are shown in Figure 4 and revealed that when loaded a fixed displacement (strain) range, the specimen showed gradually softening in the stress response. According to Figure 4b, the stress level was continuously decreasing (in absolute value) with respect to time or number of cycles, and there was no significant sign of reaching a stable value. The stress – strain loops are also shown in Figure 4c (for the first cycle) and in Figure 4d (for the full test). A small turbulence can be found in the tensile part of the loop for all cycles, which was a systematic error that came from the tensile module. The loops consistently show softening during the cyclic loading.

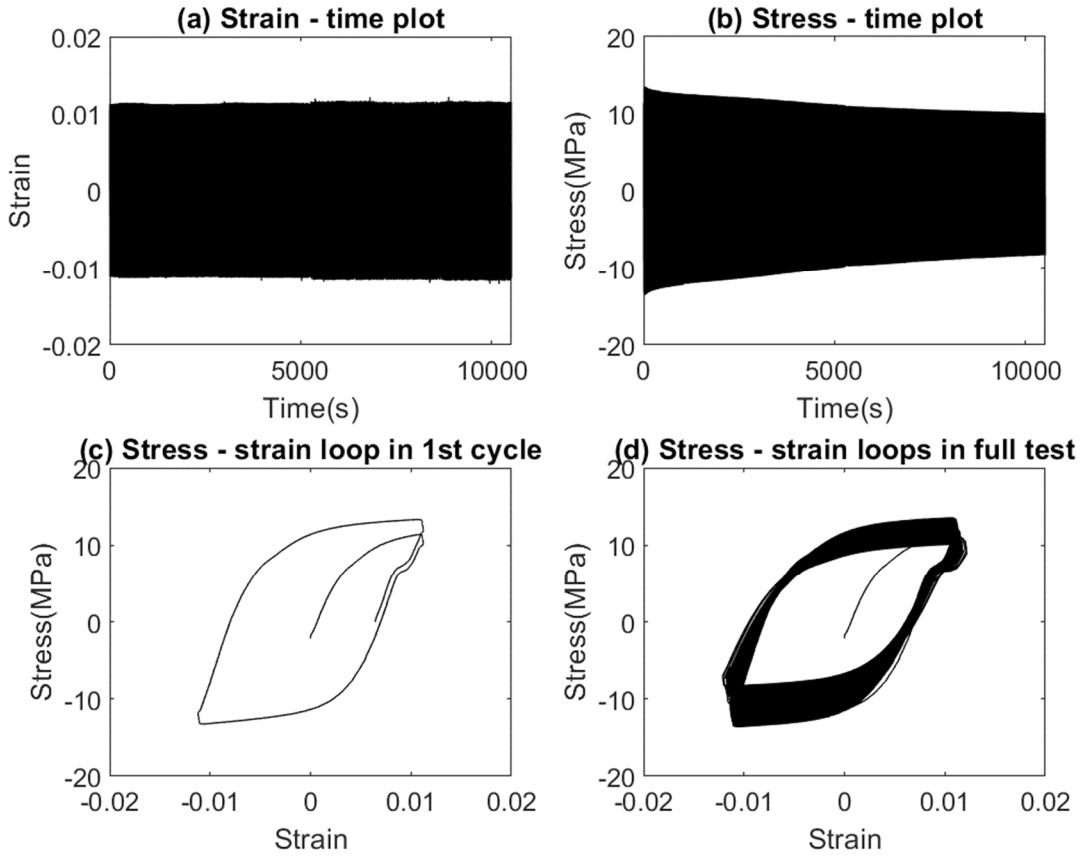

Figure 4 Mechanical testing results for the cyclic loading test. (a) strain – time plot; (b) stress – time plot; (c) stress – strain loop in 1st cycle and (d) stress – strain loops in full test.

3.2. Microstructure evolution

3.2.1 Monotonic loading

To track the microstructure evolution, the micrographs were taken by *in-situ* SEM imaging during the monotonic tensile test at 0.2 μm/s (nominal strain rate 5×10^{-5} s^{-1}). The results are divided into three stages according to different characteristics: an early stage (defined as global nominal strain from 0 to ~0.18), an intermediate stage (with global nominal strain from ~0.6 to ~0.8) and a final stage (global nominal strain from ~0.8 to ~1.1/ final failure). The SEM micrographs are presented in Figure 5 to Figure 7.

Figure 5 shows the early stage microstructure evolution during the tensile test. Before loading, the specimen showed a relatively flat and smooth topography with the presence of only some precipitates, as is also marked as a reference point in the figures. After loading, the grain boundaries first started to appear (*e.g.* the white curved segments in Figure 5b). As strain level increased, the grain boundaries became more and more significant, and some slip lines became revealed on the surface as parallel lines (indicated by parallel dashed lines inside the grains). The slip lines were mostly parallel inside one grain and were parallel neither to the loading direction nor to the transversal direction. Both the grain boundaries and the slip lines became more significant as the strain level increased. The same phenomena continued through the whole stage.

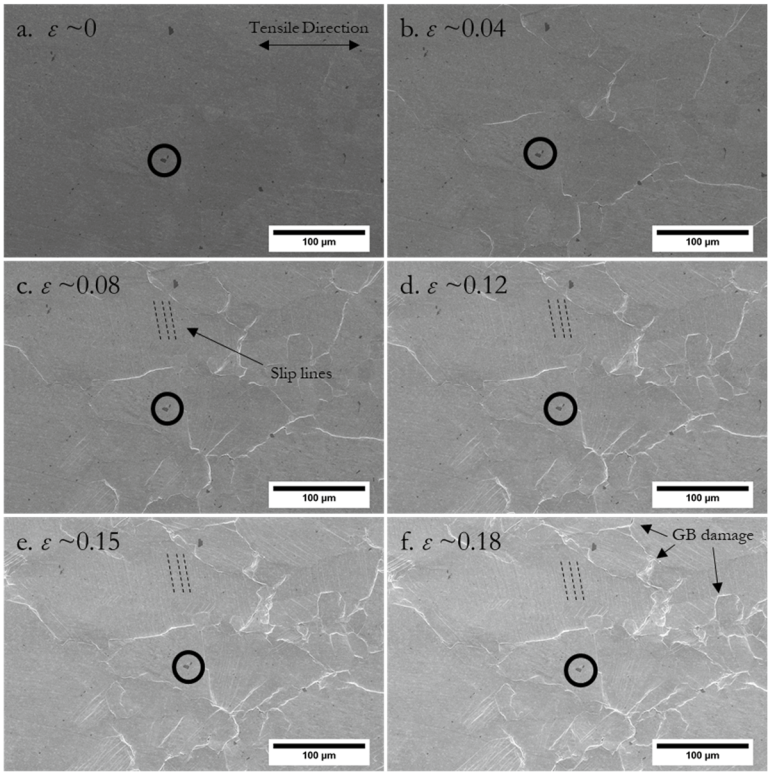

Figure 5 SEM micrographs from the *in-situ* investigation of microstructure evolution during tensile test at early stage. The corresponding global nominal strain levels are indicated in each sub-figure. The black circle indicates a same reference point in the view. The global tensile direction is horizontal.

Figure 6 shows the intermediate stage of deformation. Similar to what was observed during the early stage, the slip lines and the grain boundaries still evolved as the strain increased. Additionally, new slip lines in a different direction were observed in one grain containing previously developed slip lines. Both the new and the old slip lines were inclined to the tensile direction and the transversal direction. Moreover, the grain boundaries started to detach from each other, and early-stage damages can be found in the grain boundary areas (as indicated in Figure 6c). However, no clear proof can be found for developing damage around precipitates and/or precipitate/matrix debonding.

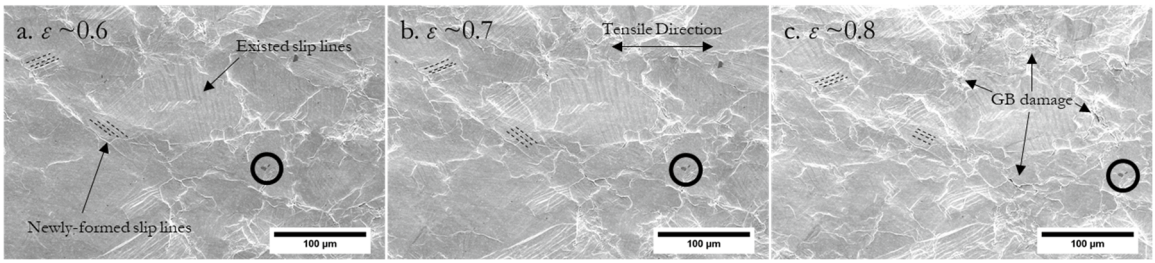

Figure 6 SEM micrographs from the *in-situ* investigation of microstructure evolution during tensile test at intermediate stage. The corresponding global nominal strain levels are indicated in each sub-figure. The black circle indicates a same reference point in the view. The global tensile direction is horizontal.

Figure 7 shows the final stage of the monotonic tensile test up to the final failure of the specimen. As observed at the end of the intermediate stage, the slip lines were inclined to the tensile direction and the transversal direction, and

the grain boundary areas were relatively severely deformed. When the material was subjected to further elongation, the slip lines turned into thicker deformation bands whose direction was almost parallel to the transversal direction (perpendicular to the tensile direction), as shown in Figure 7b. The final fracture did not start from the grain boundaries, but instead, the principal crack started from one side of the specimen in the necked area and propagated along the deformation bands in the transversal direction. From the in-situ observations, the crack was not growing in a continuous way, but accompanied with discontinuous small damage coalescence in the crack wake which finally determined the saw-tooth appearance observable at the final fracture area (Figure 7c).

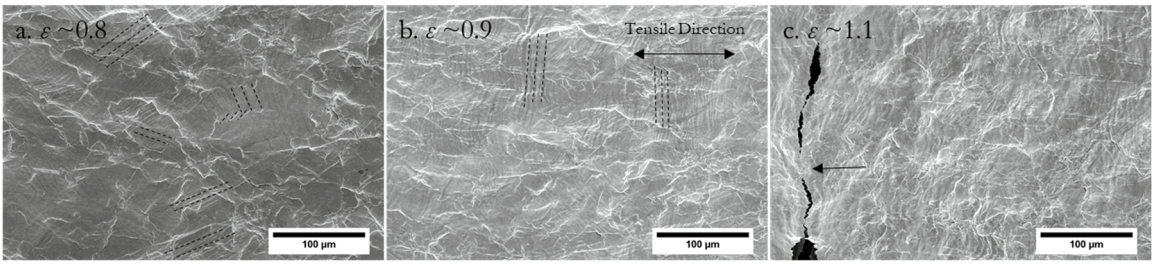

Figure 7 SEM micrographs from the *in-situ* investigation of microstructure evolution during tensile test at final stage. The corresponding global nominal strain levels are indicated in each sub-figure. The global tensile direction is horizontal.

3.2.2 Cyclic loading

The microstructure evolution during cyclic loading test was also investigated via *in-situ* imaging, analogously as was showed in the case of monotonic loading, and the results are shown in Figure 8. Unfortunately, the specimen for the cyclic loading test was not prepared by metallographic techniques due to the early-stage technical limitations. Therefore, the results here reported are to be considered as preliminary and regarded as solely qualitative. Tests with higher resolution and better sample quality are in plan and will be conducted after the Covid-19 pandemic restrictions will be released.

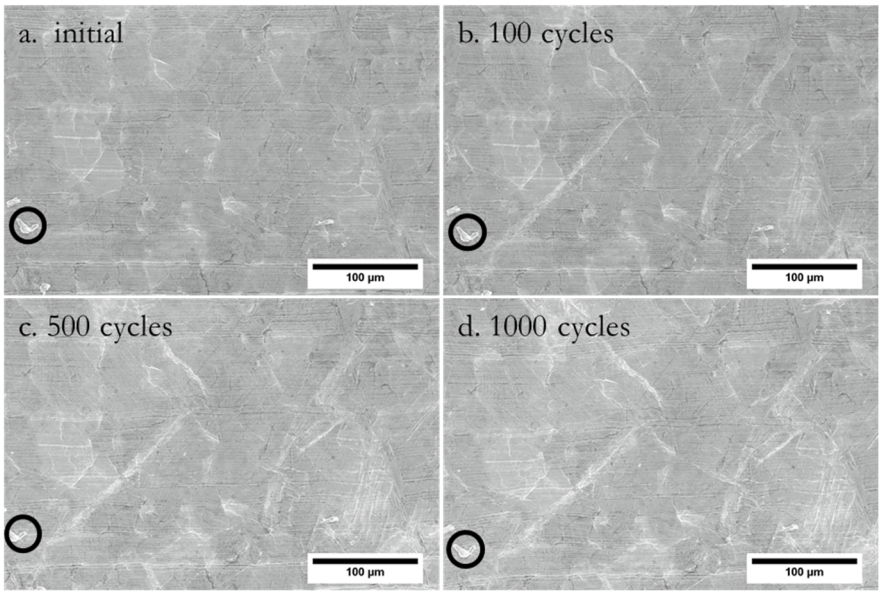

Figure 8 SEM micrographs from *the in-situ* investigation of microstructure evolution during cyclic loading test up to 1000 cycles. The black circle indicates a same reference point in the view. The global loading direction is horizontal. The horizontal lines are topographical defects from specimen manufacturing.

Similar to the early stage deformation in the monotonic tensile test, the cyclic loading showed deformation mainly appearing at grain boundaries and inside grains. Additionally, deformation bands crossing grains can also be observed. Most of the deformation bands revealed a roughly 45° angle inclination with respect to the loading direction. As the number of cycles increased, the deformation became more and more significant, but no obvious global damages were found.

4. Discussions

4.1. Monotonic tensile behavior

From the tensile testing results, an obvious strain rate sensitivity can be concluded for the studied Pb-Sn-Sb alloy. Generally, the strain rate sensitivity can be correlated to a combination of several time-dependent mechanisms occurring during deformation. Due to the relatively low melting point of Pb alloys, *i.e.* approx. 600 K, room temperature deformation for Pb alloys is similar to what is usually observed at high temperature deformation for conventional metallic materials such as aluminum or nickel. Therefore, the time-dependent procedures might have included some thermally activated deformation mechanisms such as diffusion, dislocation climbing, boundary migration, *etc*. Normally, these procedures can lead to a significant softening effect due to the fact that dislocations annihilate each other such that the global mobile dislocation density decreases. In a worse case, the damage mechanism of creep can be activated even at room temperature. These micro-mechanisms can explain the obvious strain rate sensitivity observed in the tensile tests.

The three deformation stages as described in the Results section can be linked to the dislocation slip behavior in the grains. In the first stage of early deformation, single slip systems are activated, and dislocations start to move on a specific slip plane. The result of slipping is a step on the specimen surface when dislocations slip out of the material, which is revealed as the slip lines appearing in Figure 5b-f. As the strain level increases, additional dislocations take part in the slipping procedure, and more slip lines are formed. In the same grain, the slip lines are mostly parallel in given direction, indicating that the activated slip system is limited to a specific slip plane. In this stage, the stress level also increases, indicating that activating more dislocations to slip needs higher stress level. In the intermediate stage, the slip behavior becomes more complicated: the appearance of multi-directional slip lines on the specimen's surface is indicative of a multi-slip system activation. Through the activation of different slip systems, the grains can accommodate themselves regarding the neighboring grains and the whole specimen starts to deform according to the external loading. From Figure 6, it is revealed that some grains have changed their shapes to accommodate the geometrical continuity between different grains, and the slip lines are appearing in different directions even in a same grain. In this stage, the specimen has a decreasing stress (engineering stress) level, which means that the geometrical softening becomes more dominant in the deformation process. More specifically, global necking should have already happened, according to the mechanical data. In the final stage, the different slip systems rearrange themselves to form deformation bands perpendicular to the tensile direction, as shown in Figure 7. The severely deformed region in the necked area starts to form voids which subsequently grow, more and more rapidly as elongation is further increased, until they coalesce into forming a macro-crack. The arrow in Figure 7c indicates ligament that still of the material that has not separated yet and the overall figure clearly reveal the void nucleation – growth – coalescence ductile failure mechanism typical of ductile metals.

It is however interesting to the observation that although the main topographical damages initiate and accumulate at the grain boundaries, they are not the main cause of the final failure. One possible damage accumulation at grain boundaries is initiated at lower stress/strain levels at which the deformation is completely dominated by the local microstructural features rather than the mechanical loading conditions. When the stress/ strain becomes higher, the mechanical effect overcomes the microstructural effect, such that the global deformation follows the global mechanical loading. This can be dually compared to the early stage fatigue damage evolution in cyclically loaded specimens.

Another interesting observation pertains to mechanical twinning. From the initial microstructure observation by EBSD (*i.e.* Figure 2), a lot of annealing twin boundaries can be characterized. This shows a relatively lower stacking fault energy and thus a higher twinnability of this material in the as-received conditions. Since mechanical twinning is commonly regarded as a viable method to improve both the strength and the ductility of materials during

deformation (*e.g.* twinning-induced plasticity/ TWIP steels use this criterion to improve the mechanical properties [12-16]), a deeper understanding on how mechanical twinning relates to the deformation mechanisms of the studied material can be an interesting topic. However, due to time limitation, this will be an outlook in a future work after the Covid-19 pandemic.

4.2. Cyclic loading behavior

The studied Pb-Sn-Sb alloy shows a clear cyclic softening behavior in the investigated testing range. This phenomenon is common also in some steels (*e.g.* [17, 18]), and is often explained by the reduction of dislocation density and the disappearing of sub-grain boundaries upon cyclic loading. In the present manuscript, due to time limitations, the investigation at the dislocation level was not conducted, but the microstructure evolution was revealed via *in-situ* imaging techniques. The appearance of deformation traces as observed in Figure 8 implies a dislocation slipping-dominant deformation mechanism during the cyclic loading. Since the shear stresses are most prominent at a degree of 45° to the loading direction, most of the deformation lines are along this direction, confirming the shearing nature of the deformation. However, these deformation bands are not long enough to go through the whole specimen, but rather they are limited by the obstacles present in the material. Unfortunately, it is not straightforward to identify which one of the typical metallurgical obstacles (grain boundaries, precipitates, etc.) are active due to a rough surface quality of the specimen, but based on the EBSD analysis, grain boundaries seem to be the most probable ones. Since the slip systems are defined by the crystallography of each single grain, dislocations are often slipping in different directions and on different planes when crossing grains. Therefore, most of the slip deformation cannot go through grain boundaries and will be accumulated in their vicinity. Moreover, due to the slip irreversibility during cyclic loading [19-21], only part of the deformation can be "relaxed" by the reversed dislocation motion in the "negative" half of the loading cycle. As a result, the deformation gradually and continuously accumulates at the obstacles, such as grain boundaries, and form early-stage damages and geometrical irregularities which constitute the early damage. This damage is in other words expected to add to expected creep induced void formations. Normally some extrusions/ intrusions can be observed on the surface of the specimens.

Another factor that needs to be accounted for is the fact that for this material creep damage may play a role already at room temperature in the way that during cyclic loading, the material recovers itself dynamically and the dislocation density keeps reducing (fatigue + creep interaction). To prove this hypothesis, new tests with different strain rates as well as advanced characterization techniques are needed. This is planned to be presented in a future work by the present authors.

4.3. Damage modes

Based on the investigations and the discussions, the damage modes of the studied material under the present testing conditions are summarized as follows. During monotonic tension, early-stage damage driven by microstructural constraints accumulates at grain boundaries and causes geometrical softening of the material. As stress and strain level increases, the deformation in more dominated by the global mechanical loading (Figure 9a), and final failure starts from the geometrical irregularity in the necked area and proceeds via a void coalescence mode. The final fracture is a ductile type with a locally shear type, as can be seen in Figure 9b. The fracture of the material is driven by the deformation lines as in the surrounding areas and follows a shear direction instead of the loading direction. During cyclic loading, the early-stage damages revealed as deformation lines (Figure 9c) are also controlled by the crystallography and accumulate inside the grains until an obstacle such as a grain boundary is reached. Typical extrusions/ intrusions are formed on the surface of the specimen as parallel deformation lines (Figure 9d) that can serve as geometrical irregularities, which can cause local stress concentration and a possible formation of cracks. Due to time limitation, the quantitative deformation analysis of the cyclically loaded specimen could not be completed. The possible fatigue – creep interaction is of high interest in the authors' research group and will be a topic in a future study.

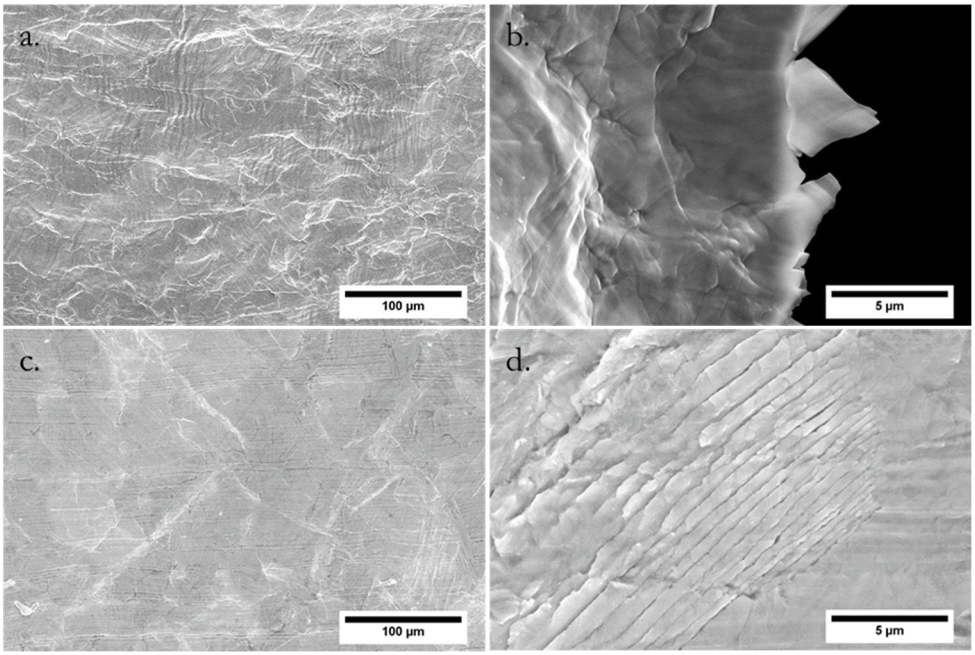

Figure 9 Damage modes micrographs. a. microstructure before failure at lower magnification (monotonic loading); b. a closer view of the final failure at higher magnification (monotonic loading); c. microstructure after cyclic loading at lower magnification (after 1000 cycles) and d. damage from cyclic loading at higher magnification (after 1000 cycles).

5. Conclusions

The tensile and fatigue behavior of a Pb-Sn-Sb alloy was investigated through small-scale mechanical testing coupled with *in-situ* imaging techniques in SEM. The tensile tests were conducted under different strain rates, and the cyclic loading test was conducted in a displacement-controlled mode at a strain amplitude of about $\Delta\varepsilon \sim \pm 1.1\%$. With the help of *in-situ* imaging, the microstructure evolution was captured during the mechanical loading. Nevertheless, the current manuscript summarizes only the preliminary results, and deeper analyses, in particular toward that of the mechanisms related to fatigue – creep interaction and dynamic recovery, will be conducted in the close future. The main conclusions from this initial investigation can be drawn as follows:

- The mechanical property of the studied Pb-Sn-Sb alloy has a strong dependency on the strain rate in the studied range (from 10^{-5} s^{-1} to 10^{-3} s^{-1}) with a clear softening phenomenon as the strain rate is decreased.
- The strain rate mainly changes the strength level (both the yielding strength and the tensile strength), while the strain to failure remains similar.
- In monotonic tensile testing, early-stage damages occur at grain boundaries, while the final failure starts from the necked area constrained by the global mechanical condition.
- The material shows a cyclic softening behavior when subjected to cyclic loading, and the formation of extrusions/ intrusions as a result of persistent slip bands is observed.
- Dynamic recovery can be a possible mechanism for both monotonic loading and cyclic loading. This is the outlook of the present work and will be conducted in the close future.

Acknowledgements

The authors would like to thank the financial support from Nexans Norway AS and the Research Council of Norway (IPN in ENERGIX, Project number 256367) and performed within the project: Next-generation damage based fatigue of cable sheathing (REFACE).

References

[1] A. Johanson, L.M. Viespol, A. Alvaro, F. Berto, Small- and Full-Scale Fatigue Testing of Lead Cable Sheathing, The 29th International Ocean and Polar Engineering Conference, International Society of Offshore and Polar Engineers, Honolulu, Hawaii, USA, 2019, p. 6.
[2] L.M. Viespoli, A. Johanson, A. Alvaro, B. Nyhus, F. Berto, Room temperature creep mechanism of a Pb-Sn-Sb lead alloy, Procedia Structural Integrity 18 (2019) 86-92.
[3] H.F. Moore, N.J. Alleman, The creep of lead and lead alloys used for cable sheathing, University of Illinois at Urbana Champaign, College of Engineering, 1932.
[4] C.W. Dollins, C.E. Betzer, Creep, fracture, and bending of lead and lead alloy cable sheathing, University of Illinois at Urbana Champaign, College of Engineering, 1956.
[5] P. Feltham, On the Mechanism of High-Temperature Creep in Metals with Special Reference to Polycrystalline Lead, Proceedings of the Physical Society. Section B 69(12) (1956) 1173-1188.
[6] D. Harvard, Fatigue of Lead Cable-Sheathing Alloys, Ontario Hydro research (1972).
[7] P. Anelli, F. Donazzi, W. Lawson, The fatigue life of lead alloy E as a sheathing material for submarine power cables, IEEE Transactions on power delivery 3(1) (1988) 69-75.
[8] M.K. Sahota, J.R. Riddington, Compressive creep properties of lead alloys, Mater. Des. 21(3) (2000) 159-167.
[9] A. Johanson, L.M. Viespoli, B. Nyhus, A. Alvaro, F. Berto, Experimental and numerical investigation of strain distribution of notched lead fatigue test specimen, 12th International Fatigue Congress (Fatigue 2018) 165 (2018).
[10] L.M. Viespoli, A. Johanson, A. Alvaro, B. Nyhus, F. Berto, Strain controlled medium cycle fatigue of a notched Pb-Sn-Cd lead alloy, Engineering Failure Analysis 104 (2019) 96-104.
[11] L.M. Viespoli, A. Johanson, A. Alvaro, B. Nyhus, A. Sommacal, F. Berto, Tensile characterization of a lead alloy: creep induced strain rate sensitivity, Mater. Sci. Eng., A 744 (2019) 365-375.
[12] O. Grässel, L. Krüger, G. Frommeyer, L.W. Meyer, High strength Fe–Mn–(Al, Si) TRIP/TWIP steels development — properties — application, Inter. J. Plast. 16(10-11) (2000) 1391-1409.
[13] O. Bouaziz, N. Guelton, Modelling of TWIP effect on work-hardening, Mater. Sci. Eng., A 319-321 (2001) 246-249.
[14] S. Allain, J.P. Chateau, O. Bouaziz, A physical model of the twinning-induced plasticity effect in a high manganese austenitic steel, Mater. Sci. Eng., A 387-389 (2004) 143-147.
[15] S.-J. Lee, J. Kim, S.N. Kane, B.C.D. Cooman, On the origin of dynamic strain aging in twinning-induced plasticity steels, Acta Mater. 59(17) (2011) 6809-6819.
[16] B.C. De Cooman, Y. Estrin, S.K. Kim, Twinning-induced plasticity (TWIP) steels, Acta Mater. 142 (2018) 283-362.
[17] P. Sulich, W. Egner, S. Mroziński, H. Egner, Modeling of cyclic thermo-elastic-plastic behaviour of P91 steel, Journal of Theoretical and Applied Mechanics (2017).
[18] M.F. Giordana, P.F. Giroux, I. Alvarez-Armas, M. Sauzay, A. Armas, Micromechanical modeling of the cyclic softening of EUROFER 97 steel, Procedia Engineering 10 (2011) 1268-1273.
[19] H. Mughrabi, Dislocation wall and cell structures and long-range internal stresses in deformed metal crystals, Acta Metall. 31(9) (1983) 1367-1379.
[20] H. Mughrabi, Cyclic Slip Irreversibilities and the Evolution of Fatigue Damage, Metallurgical and Materials Transactions B 40(4) (2009) 431-453.
[21] H. Mughrabi, Cyclic slip irreversibility and fatigue life: A microstructure-based analysis, Acta Mater. 61(4) (2013) 1197-1203.